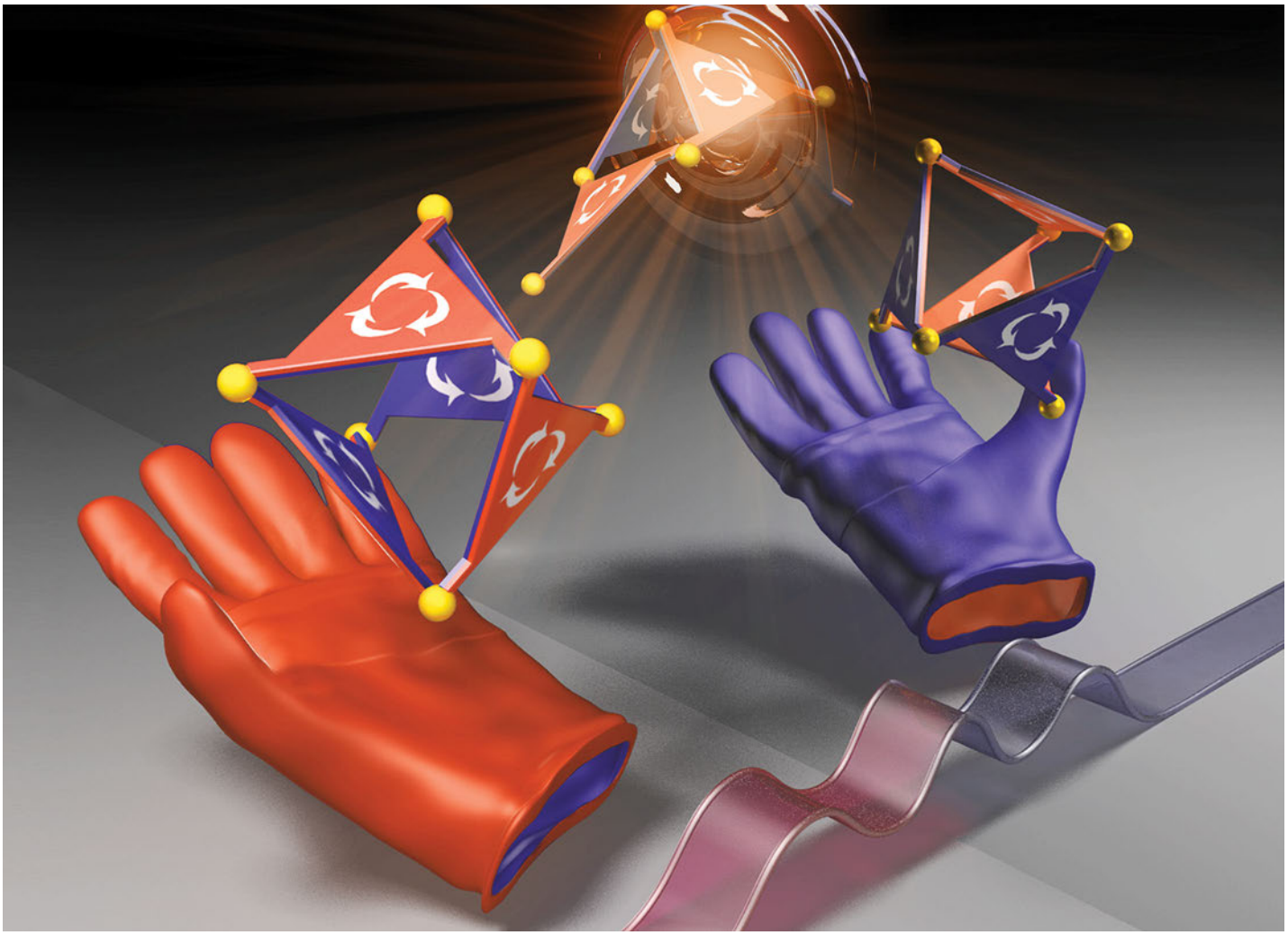

Showcasing research from Xiao-Yu Cao's laboratory, Department of Chemistry, Xiamen University, China.

Interconversion of molecular face-rotating polyhedra through turning inside out

Chiral organic cages with face-rotating patterns can interconvert to their enantiomers through turning inside out. This specific interconversion strategy is similar to switching the chirality of a rubber glove. Kinetics investigation reveals that the turn-inside-out interconversion is realized through the partial disassembly of the cage.

As featured in:

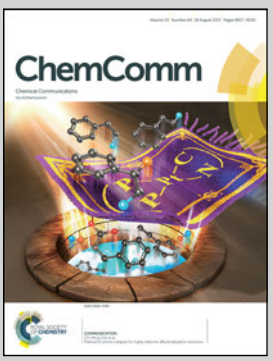

See Xiaoyu Cao *et al.*, *Chem. Commun.*, 2017, **53**, 8956.

ROYAL SOCIETY OF CHEMISTRY

rsc.li/chemcomm

Registered charity number: 207890

ChemComm

COMMUNICATION

View Article Online
View Journal | View Issue

Cite this: *Chem. Commun.*, 2017, 53, 8956

Received 29th May 2017,
Accepted 13th June 2017

DOI: 10.1039/c7cc04159d

rsc.li/chemcomm

Interconversion of molecular face-rotating polyhedra through turning inside out†

Yu Wang,[ab] Hongxun Fang,[a] Wei Zhang,[ab] Yongbin Zhuang,[a] Zhongqun Tian[a] and Xiaoyu Cao*[a]

We report the post-synthesis interconversion of two enantiomeric organic cages through turning inside out. By scrutinizing the thermodynamics and kinetics, we are able to control the racemization rate by various reaction conditions and reveal that the turning-inside-out interconversion is realized through a partial disassembly pathway. The kinetics investigation also provides insight into the dynamic essence of imine chemistry using different solvents and catalysts.

Chiral cage compounds have received considerable attention due to their importance for enantioselective recognition and separations,[1–3] as asymmetric catalysts,[4–9] and as a tool to illustrate how chirality emerges.[10,11] Using hydrogen bonds,[12,13] metal-organic coordination[14–18] and dynamic covalent bonds,[19–22] scientists have constructed many cages with various types of chirality (*e.g.*, rooted in chiral carbon,[20,23] chiral-at-metal,[24,25] asymmetric faces,[26] axial chirality[27] and inherent chirality).[12,28] Despite there being many methods for constructing chiral cages, only a few strategies have been developed to regulate the chirality of cages after their formation, which are mainly achieved through the racemization and isomerization processes.[29–32] Some cases (*e.g.*, for asymmetric catalysts)[33,34] require non-racemizing chiral cages, whereas other cases (*e.g.*, for chiral switches[35–37]) prefer chiral cages that can rapidly change their chirality. To endow chiral cages with suitable rates of racemization or isomerization, insights into the kinetics and pathways of these processes are desired. Such rules can guide to more robust cages for catalysis[6] and stimuli-responsive materials with controllable chirality,[38–40] and may have implications for the understanding of the supramolecular racemization processes in life sciences.[41]

Racemization of chiral cages is mainly realized in metal-organic systems through the Δ/Λ isomerization of metal centers.[42–44] Systematical studies on the racemization and isomerization of metal-organic cages have promoted their applications in complex chemical systems.[33,45,46] Chiral organic cages, by contrast, are mainly assembled from building blocks with chiral carbon centers,[1,20] which can hardly undergo the racemization or isomerization process. A few chiral organic cages have been assembled from achiral building blocks,[12,13,22,47] however, the difficulty in isolating racemic enantiomers has hindered the exploration of the racemization mechanism of organic cages.

Recently, we developed a strategy to construct chiral face-rotating polyhedra from achiral vertices and two-dimensional chiral faces through dynamic covalent chemistry.[26] C_{3h}-symmetric truxene (TR) building blocks and ethylenediamine (EDA) were assembled into two racemic enantiomers in a tetra-capped octahedral structure (Fig. 1a). Each truxene unit of the octahedra exhibits two opposite rotational directionalities on either the exterior or interior faces, as shown by the blue clockwise (C) and red anti-clockwise (A) arrows in Fig. 1a and b. Hence, the enantiomers are named after the directionalities of the exterior faces as (CCCC)-**1** and (AAAA)-**1**.

Herein, we report a finding that the isolated (CCCC)-**1** and (AAAA)-**1** can interconvert to their enantiomers through a unique turn-inside-out strategy (Fig. 1b). This specific interconversion strategy is similar to switching the chirality of a rubber glove by turning inside out (Fig. 1c), and is unprecedented for cage compounds. Besides, to our knowledge, this is also the first supramolecular racemization process that is achieved through dynamic covalent chemistry.[48,49] We investigate the racemization of (AAAA)-**1** under various reaction conditions and further reveal the interconversion mechanism by monitoring the racemization kinetics and performing the corresponding theoretical deduction.

The (CCCC)-**1** and (AAAA)-**1** enantiomers were separated by chiral high-performance liquid chromatography (HPLC) in the mobile phase of hexane and ethyl acetate, using Daicel Chiralcel IE Columns. When dissolved in toluene, the isolated (CCCC)-**1** and (AAAA)-**1** presented mirror-like CD spectra with strong intensities at the peak of 340 nm (Fig. S1, ESI†), showing a negligible decrease in 24 hours at room temperature (298 K). This suggests that the truxene cage is more rigid than the structurally resembled [4 + 6]

[a] *State Key Laboratory of Physical Chemistry of Solid Surfaces, iChEM and College of Chemistry and Chemical Engineering, Xiamen University, Xiamen 361005, China. E-mail: xcao@xmu.edu.cn; Fax: +86-592-2186628; Tel: +86-592-2183098*
[b] *Department of Polymer Science, College of Polymer Science and Polymer Engineering, The University of Akron, Akron, Ohio 44325, USA*

† Electronic supplementary information (ESI) available. See DOI: 10.1039/c7cc04159d

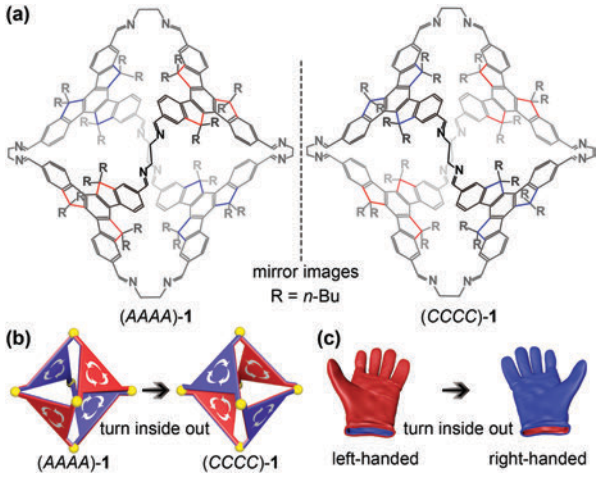

Fig. 1 (a) Molecular structures of face-rotating octahedra (CCCC)-**1** and (AAAA)-**1**. Rotation patterns along the three sp^3 carbons of the truxene face are considered to be either clockwise (C) or anticlockwise (A) when viewed from outside or inside of the octahedra, as indicated by the blue (C) and red (A) arrows. Configurations of the octahedral enantiomers are named after the directionalities of the exterior faces as (CCCC)-**1** and (AAAA)-**1**. (b) Schematic of converting (CCCC)-**1** to its enantiomeric (AAAA)-**1** through turning the octahedron inside out. (c) Schematic of converting a left-handed rubber glove to a right-handed one through turning it inside out.

imine cage reported by Cooper *et al.*[35,36,47] despite being much larger.

Nevertheless, when a solution of enantiomers was heated at 60 °C with 5% TFA as a catalyst, a distinct decrease in the CD intensity was found in 5 hours for both (CCCC)-**1** and (AAAA)-**1** (Fig. 2a and b). Mass spectrometry analysis indicated that the enantiomers retained their cage structure (Fig. S2, ESI†). HPLC analysis further confirmed the racemization process and the concurrent generation of a small amount of a TR monomer (Fig. 2c and d).

To determine the racemization kinetics, (AAAA)-**1** was racemized at various temperatures and characterized by time-dependent CD spectroscopy. This result showed that the CD intensity decreased

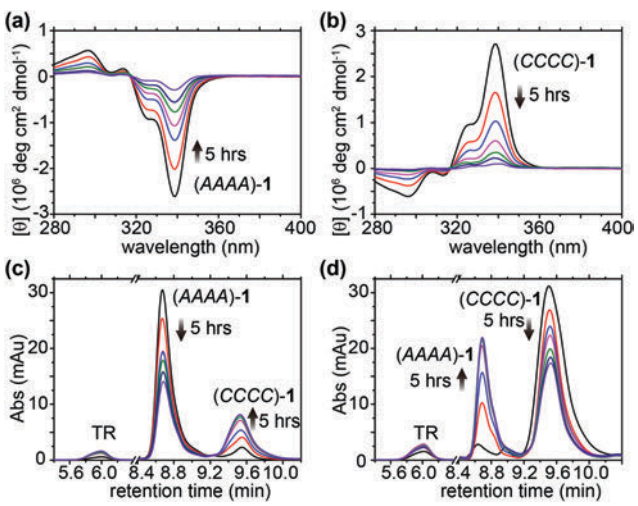

Fig. 2 CD spectra (a and b) and HPLC spectra (c and d) during the racemization of (AAAA)-**1** and (CCCC)-**1** in toluene at a temperature of 333 K.

with time in an exponential manner and the decreasing rate increased with an increase of temperature (Fig. 3a). In other words, ln[CD] decreased linearly with time and the slopes became more negative when the temperature increased (Fig. 3b), suggesting the first-order kinetics of racemization.[50] Nevertheless, the racemization of (AAAA)-**1** essentially contains two opposing reactions, *i.e.*, the forward reaction from (AAAA)-**1** to (CCCC)-**1** and the reverse reaction from (CCCC)-**1** to (AAAA)-**1**, as shown in eqn (1)

$$\begin{gathered}\text{(AAAA)-}\mathbf{1} \xrightarrow{k_{obs}} \text{(CCCC)-}\mathbf{1} \\ \text{(AAAA)-}\mathbf{1} \underset{k_{-1}}{\overset{k_1}{\rightleftharpoons}} \text{(CCCC)-}\mathbf{1},\end{gathered} \tag{1}$$

in which k_{obs} is the observed rate constant of the racemization, and k_1 and k_{-1} are the rate constants of the forward and reverse reactions, respectively. Deduction of the racemization kinetics based on eqn (1) (see details in the ESI†) gives relationships between the CD intensity and racemization time: $\ln[CD] = -k_{obs}t$ and $k_{obs} = 2k_1$.

Using the Erying equation ($\ln(k/T) = -\Delta H^{\ddagger}/(RT) + \ln(k_B/h) + \Delta S^{\ddagger}/R$) to fit the kinetics of the forward and reverse conversions at different temperatures (Fig. 3c and Table S1, ESI†), we obtained the kinetic parameters: $\Delta H^{\ddagger}_{obs} = 94.3\ \text{kJ mol}^{-1}$ and $S^{\ddagger}_{obs} = -35.2\ \text{J mol}^{-1}\ \text{K}^{-1}$ for the observed racemization; $\Delta H^{\ddagger}_{1} = \Delta H^{\ddagger}_{-1} = 94.3\ \text{kJ mol}^{-1}$ and $\Delta S^{\ddagger}_{1} = \Delta S^{\ddagger}_{-1} = -41.0\ \text{J mol}^{-1}\ \text{K}^{-1}$ for the forward and reverse reactions. Using these parameters, we calculated the rate constant and half-life at room temperature (298 K) to be $k_{obs} = 2.6 \times 10^{-6}\ \text{s}^{-1}$ and $t_{1/2} = 74$ h, explaining why we hardly observed the racemization at room temperature.

The kinetics investigation of this racemizing system can also help to reveal the dynamic essences of imine chemistry.[51–53] The excellent spectroscopic sensitivity and HPLC separability of this racemizing system allow us to investigate the kinetics

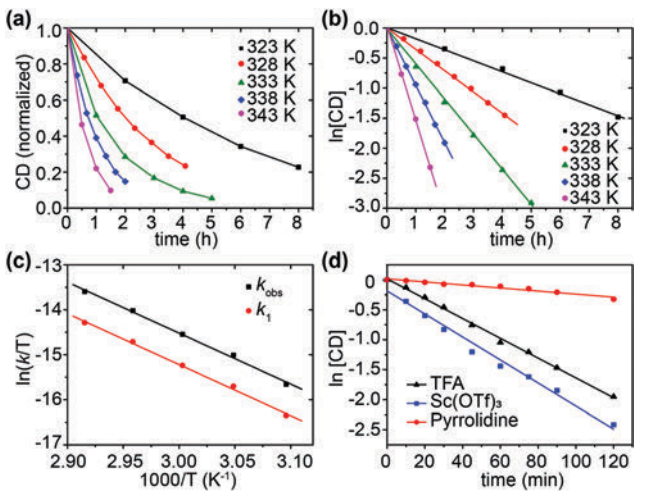

Fig. 3 (a) Normalized CD intensity and (b) logarithm of the CD intensity *versus* the reaction time during the racemization of (AAAA)-**1** in toluene at a concentration of 100 μM at various temperatures. (c) Rate constants at different temperatures fitted by the Eyring equation. (d) Logarithm of the normalized CD intensity *versus* the reaction time during the racemization of (AAAA)-**1** (100 μM, 338 K) in toluene with different catalysts (5 μM).

under various reaction conditions for understanding the influence of solvents and catalysts. For example, we compared three typical kinds of catalysts for imine chemistry (Fig. 3d and Fig. S3, ESI†). TFA and the Sc^{3+} ion[54] showed a similar efficiency for the cage racemization, whereas pyrrolidine[55] has a relatively lower efficiency. And as a comparison, the (AAAA)-**1** enantiomer exhibited a high stability and showed no decrease of the CD intensity in toluene at 338 K without the presence of a catalyst (Fig. S3, ESI†). In another example, we investigate the racemization kinetics in dichloromethane (DCM) through a similar approach as in toluene. As two common solvents of dynamic covalent chemistry, DCM leads to a much faster racemization than toluene (Fig. S4 and Table S2, ESI†). The racemization of 100 μM (AAAA)-**1** in DCM can take place at room temperature (298 K) with 5% TFA, and the calculated activation enthalpy is much smaller than that in toluene: $\Delta H^{\ddagger}_{obs}(\mathrm{DCM}) = 61.9\ \mathrm{kJ\ mol^{-1}}$ and $S^{\ddagger}_{obs}(\mathrm{DCM}) = -118.5\ \mathrm{J\ mol^{-1}\ K^{-1}}$.

The kinetics investigation allows us to further understand the pathway of racemization. The racemization kinetics were dramatically influenced by the catalysts for imine chemistry, suggesting that the racemization pathway contains the cleavage and the reunion of imine bonds.[53] As the cage enantiomers were constructed from TR and ethylenediamine (EDA) monomers, and a small amount of a TR monomer was generated during the racemization, one might presume that the interconversion was realized through a complete disassembly pathway (path 1 in Fig. 4a), in which (AAAA)-**1** first completely disassembles into TR and EDA monomers and then the monomers reassemble into (CCCC)-**1**. The energy coordinate of this complete disassembly pathway (dashed line in Fig. 4b) contains two activation energy barriers: the larger one $\left(\Delta G^{\ddagger}_{1}\right)$ corresponding to the complete disassembly step and the smaller one $\left(\Delta G^{\ddagger}_{2}\right)$ corresponding to the reassembly step. $\Delta G^{\ddagger}_{1}$ is equal to the sum of $\Delta G^{\ddagger}_{2}$ and ΔG_3, where ΔG_3 represents the energy difference between cage **1** and the building blocks and is calculated to be 61.8 kJ mol^{-1} by analysing the equilibrium distributions of cage **1** and the TR monomer (Fig. S5 and Table S3, ESI†). To evaluate $\Delta G^{\ddagger}_{2}$, we performed a parallel kinetics investigation of the synthesis of cage **1** and the racemization of (AAAA)-**1** under the same conditions. As shown in Fig. S6 (ESI†), the assembly from building blocks to cage **1** progressed much slower than the racemization of (AAAA)-**1** at the same concentration and temperature. This indicates that even $\Delta G^{\ddagger}_{2}$ itself is larger than the observed overall activation energy of racemization, *i.e.*, $\Delta G^{\ddagger}_{obs,343K} = 106\ \mathrm{kJ\ mol^{-1}}$. Therefore, $\Delta G^{\ddagger}_{path1}$ is much larger than the $\Delta G^{\ddagger}_{obs,343K}$, suggesting that the racemization is not mainly realized through the complete disassembly pathway.

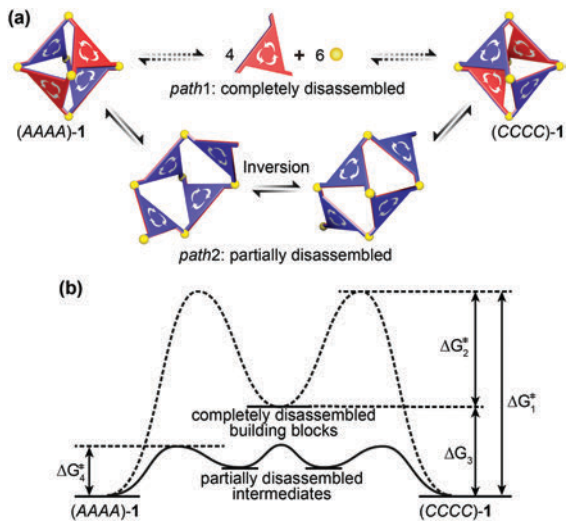

Fig. 4 (a) Two proposed reaction pathways of the interconversion between (AAAA)-**1** and (CCCC)-**1**. The dashed arrow represents the pathway through completely disassembled building blocks, *i.e.*, the truxene monomer and EDA. The solid arrow represents the pathway through partially disassembled concave intermediates, involving the cleavage and reunion of one imine bond. (b) Reaction coordinates of the complete disassembly pathway (dashed line) and the partial disassembly pathway (solid line).

By contrast, the partial disassembly pathway seems to be in accordance with the racemization kinetics (path 2 in Fig. 4a). After cleavage of one imine bond, the cage is opened and becomes a bowl-like concave intermediate. Given the conformational flexibility of the concave intermediate and in particular the EDA bridges, subsequent pushing of the central node through the cavity all the way to the opposite side would realize the inversion in a similar way to the racemization of many concave molecules.[56,57] The cleavage of fewer diamine bonds in the partial disassembly pathway results in a much lower activation energy barrier than that through the complete disassembly pathway (Fig. 4b). Note that, because of the dynamic nature of DCC,[48,49] the racemization pathway would not likely be an exclusive one;[58] hence, other partial disassembly pathways might also contribute to the racemization (Fig. S7, ESI†). And also because of the dynamic nature of DCC, the constitutional library at the equilibrium state inevitably contains minor amounts of amines and aldehyde building blocks for a dynamic imine chemistry.[52] As a result, the equilibrium states for either the synthesis or the racemization of cage **1** are the same, both of which contain *ca.* 3% TR monomer (Fig. S5, ESI†). This explains why we observed a small amount of the TR monomer during the racemization process, although the racemization was mainly achieved through a partial disassembly pathway (as detailed in Fig. S8, ESI†).

To summarize, we have demonstrated the racemization of an organic cage through a novel turning-inside-out mechanism. The racemization kinetics was analyzed by CD spectroscopy and HPLC at various temperatures, solvents and catalysts. Combining the kinetics investigation and the theoretical deduction, we reason that the racemization was achieved by turning the cage inside out through a partial disassembly pathway. This study provides insights into the post-synthesis regulation of cage chirality and benefits the in-depth understanding of dynamic covalent chemistry. It may facilitate the design of large and rigid cages that do not interconvert the chirality in the absence of acid catalysts, and also the construction of more cages with switchable chirality for chiral recognition, asymmetric catalysis and as smart chiral materials.

References

1 L. Chen, P. S. Reiss, S. Y. Chong, D. Holden, K. E. Jelfs, T. Hasell, M. A. Little, A. Kewley, M. E. Briggs, A. Stephenson, K. M. Thomas, J. A. Armstrong, J. Bell, J. Busto, R. Noel, J. Liu, D. M. Strachan, P. K. Thallapally and A. I. Cooper, *Nat. Mater.*, 2014, **13**, 954–960.
2 W. Xuan, M. Zhang, Y. Liu, Z. Chen and Y. Cui, *J. Am. Chem. Soc.*, 2012, **134**, 6904–6907.
3 K. Wu, K. Li, Y.-J. Hou, M. Pan, L.-Y. Zhang, L. Chen and C.-Y. Su, *Nat. Commun.*, 2016, **7**, 10487.
4 M. D. Pluth, R. G. Bergman and K. N. Raymond, *Science*, 2007, **316**, 85–88.
5 D. M. Kaphan, M. D. Levin, R. G. Bergman, K. N. Raymond and F. D. Toste, *Science*, 2015, **350**, 1235–1238.
6 C. J. Brown, F. D. Toste, R. G. Bergman and K. N. Raymond, *Chem. Rev.*, 2015, **115**, 3012–3035.
7 J. Meeuwissen and J. N. Reek, *Nat. Chem.*, 2010, **2**, 615–621.
8 Q. Han, C. He, M. Zhao, B. Qi, J. Niu and C. Duan, *J. Am. Chem. Soc.*, 2013, **135**, 10186–10189.
9 P. Howlader, P. Das, E. Zangrando and P. S. Mukherjee, *J. Am. Chem. Soc.*, 2016, **138**, 1668–1676.
10 W. Meng, T. K. Ronson and J. R. Nitschke, *Proc. Natl. Acad. Sci. U. S. A.*, 2013, **110**, 10531–10535.
11 D. Beaudoin, F. Rominger and M. Mastalerz, *Angew. Chem., Int. Ed.*, 2017, **56**, 1244–1248.
12 D. Ajami and J. J. Rebek, *Nat. Chem.*, 2009, **1**, 87–90.
13 L. R. MacGillivray and J. L. Atwood, *Nature*, 1997, **389**, 469–472.
14 T. R. Cook and P. J. Stang, *Chem. Rev.*, 2015, **115**, 7001–7045.
15 T. R. Cook, Y.-R. Zheng and P. J. Stang, *Chem. Rev.*, 2013, **113**, 734–777.
16 M. D. Ward and P. R. Raithby, *Chem. Soc. Rev.*, 2013, **42**, 1619–1636.
17 Y. Inokuma, M. Kawano and M. Fujita, *Nat. Chem.*, 2011, **3**, 349–358.
18 L.-L. Yan, C.-H. Tan, G.-L. Zhang, L.-P. Zhou, J.-C. Bunzli and Q.-F. Sun, *J. Am. Chem. Soc.*, 2015, **137**, 8550–8555.
19 A. G. Slater and A. I. Cooper, *Science*, 2015, **348**, aaa8075.
20 G. Zhang and M. Mastalerz, *Chem. Soc. Rev.*, 2014, **43**, 1934–1947.
21 Y. Jin, Q. Wang, P. Taynton and W. Zhang, *Acc. Chem. Res.*, 2014, **47**, 1575–1586.
22 J. Sun, J. L. Bennett, T. J. Emge and R. Warmuth, *J. Am. Chem. Soc.*, 2011, **133**, 3268–3271.
23 K. E. Jelfs, X. Wu, M. Schmidtmann, J. T. A. Jones, J. E. Warren, D. J. Adams and A. I. Cooper, *Angew. Chem., Int. Ed.*, 2011, **50**, 10653–10656.
24 A. M. Castilla, W. J. Ramsay and J. R. Nitschke, *Acc. Chem. Res.*, 2014, **47**, 2063–2073.
25 M. M. J. Smulders, I. A. Riddell, C. Browne and J. R. Nitschke, *Chem. Soc. Rev.*, 2013, **42**, 1728–1754.
26 X. Wang, Y. Wang, H. Yang, H. Fang, R. Chen, Y. Sun, N. Zheng, K. Tan, X. Lu, Z. Tian and X. Cao, *Nat. Commun.*, 2016, **7**, 12469.
27 Y. Ye, T. R. Cook, S.-P. Wang, J. Wu, S. Li and P. J. Stang, *J. Am. Chem. Soc.*, 2015, **137**, 11896–11899.
28 A. Szumna, *Chem. Soc. Rev.*, 2010, **39**, 4274–4285.
29 L. J. Prins, F. De Jong, P. Timmerman and D. N. Reinhoudt, *Nature*, 2000, **408**, 181–184.
30 T. Ishi-i, M. Crego-Calama, P. Timmerman, D. N. Reinhoudt and S. Shinkai, *J. Am. Chem. Soc.*, 2002, **124**, 14631–14641.
31 M. Kieffer, B. S. Pilgrim, T. K. Ronson, D. A. Roberts, M. Aleksanyan and J. R. Nitschke, *J. Am. Chem. Soc.*, 2016, **138**, 6813–6821.
32 N. Ousaka, S. Grunder, A. M. Castilla, A. C. Whalley, J. F. Stoddart and J. R. Nitschke, *J. Am. Chem. Soc.*, 2012, **134**, 15528–15537.
33 A. M. Castilla, N. Ousaka, R. A. Bilbeisi, E. Valeri, T. K. Ronson and J. R. Nitschke, *J. Am. Chem. Soc.*, 2013, **135**, 17999–18006.
34 Z. J. Wang, K. N. Clary, R. G. Bergman, K. N. Raymond and F. D. Toste, *Nat. Chem.*, 2013, **5**, 100–103.
35 J. T. A. Jones, D. Holden, T. Mitra, T. Hasell, D. J. Adams, K. E. Jelfs, A. Trewin, D. J. Willock, G. M. Day and J. Bacsa, *et al.*, *Angew. Chem., Int. Ed.*, 2011, **50**, 749–753.
36 K. E. Jelfs, F. Schiffmann, J. T. A. Jones, B. Slater, F. Cora and A. I. Cooper, *Phys. Chem. Chem. Phys.*, 2011, **13**, 20081–20085.
37 K. Shimomura, T. Ikai, S. Kanoh, E. Yashima and K. Maeda, *Nat. Chem.*, 2014, **6**, 429–434.
38 A. J. McConnell, C. S. Wood, P. P. Neelakandan and J. R. Nitschke, *Chem. Rev.*, 2015, **115**, 7729–7793.
39 Z. He, W. Jiang and C. A. Schalley, *Chem. Soc. Rev.*, 2015, **44**, 779–789.
40 L. You, D. Zha and E. V. Anslyn, *Chem. Rev.*, 2015, **115**, 7840–7892.
41 T. Geiger and S. Clarke, *J. Biol. Chem.*, 1987, **262**, 785–794.
42 A. J. Terpin, M. Ziegler, D. W. Johnson and K. N. Raymond, *Angew. Chem., Int. Ed.*, 2001, **40**, 157–160.
43 S. Alvarez, *Chem. Rev.*, 2015, **115**, 13447–13483.
44 T. Imamura, T. Maehara, R. Sekiya and T. Haino, *Chem. – Eur. J.*, 2016, **22**, 3250–3254.
45 A. V. Davis, T. K. Firman, B. P. Hay and K. N. Raymond, *J. Am. Chem. Soc.*, 2006, **128**, 9484–9496.
46 S. Zarra, D. M. Wood, D. A. Roberts and J. R. Nitschke, *Chem. Soc. Rev.*, 2015, **44**, 419–432.
47 J. T. A. Jones, T. Hasell, X. Wu, J. Bacsa, K. E. Jelfs, M. Schmidtmann, S. Y. Chong, D. J. Adams, A. Trewin and F. Schiffman, *et al.*, *Nature*, 2011, **474**, 367–371.
48 S. J. Rowan, S. J. Cantrill, G. R. Cousins, J. K. Sanders and J. F. Stoddart, *Angew. Chem., Int. Ed.*, 2002, **41**, 898–952.
49 J.-M. Lehn, *Chem. Soc. Rev.*, 2007, **36**, 151–160.
50 P. Atkins and J. de Paule, *Atkins' Physcial Chemistry*, Oxford University Press, Oxford, 8th edn, 2006.
51 J.-M. Lehn, *Chem. Soc. Rev.*, 2007, **36**, 151–160.
52 M. E. Belowich and J. F. Stoddart, *Chem. Soc. Rev.*, 2012, **41**, 2003–2024.
53 P. Kovaricek and J.-M. Lehn, *J. Am. Chem. Soc.*, 2012, **134**, 9446–9455.
54 N. Giuseppone, J.-L. Schmitt, E. Schwartz and J.-M. Lehn, *J. Am. Chem. Soc.*, 2005, **127**, 5528–5539.
55 S. Morales, F. G. Guijarro, J. L. Garcia Ruano and M. B. Cid, *J. Am. Chem. Soc.*, 2014, **136**, 1082–1089.
56 A. Szumna, *Chem. Soc. Rev.*, 2010, **39**, 4274–4285.
57 T. Kusano, M. Tabatabai, Y. Okamoto and V. Böhmer, *J. Am. Chem. Soc.*, 1999, **121**, 3789–3790.
58 N. Ponnuswamy, F. B. Cougnon, J. M. Clough, G. D. Pantos and J. K. Sanders, *Science*, 2012, **338**, 783–785.